

Article

Raman Laser Spectrometer: Application to $^{12}\text{C}/^{13}\text{C}$ Isotope Identification in CH_4 and CO_2 Greenhouse Gases

Vladimir Vitkin ¹, Anton Polishchuk ¹, Ian Chubchenko ¹ , Evgeniy Popov ¹,
Konstantin Grigorenko ¹ , Artem Kharitonov ¹, Arsen Davtian ¹, Anton Kovalev ¹ ,
Valeria Kurikova ¹, Patrice Camy ², Pavel Loiko ² , Magdalena Aguiló ³, Francesc Díaz ³ and
Xavier Mateos ^{3,*}

¹ ITMO University, 49 Kronverksky Pr., 197101 St. Petersburg, Russia; v.v.v@bk.ru (V.V.); ap1994@mail.ru (A.P.); Chubchenko.ian@itmo.ru (I.C.); eepopov@itmo.ru (E.P.); kmgrigor@itmo.ru (K.G.); aakharitovov@itmo.ru (A.K.); asdavian@itmo.ru (A.D.); avkovalev@niuitmo.ru (A.K.); korninec@mail.ru (V.K.)

² Centre de Recherche sur les Ions, les Matériaux et la Photonique (CIMAP), UMR 6252 CEA-CNRS-ENSICAEN, Université de Caen, 6 Boulevard du Maréchal Juin, 14050 Caen, France; patrice.camy@ensicaen.fr (P.C.); pavel.loiko@ensicaen.fr (P.L.)

³ Universitat Rovira i Virgili (URV), Física i Cristal·lografia de Materials i Nanomaterials (FiCMA-FiCNA)-EMaS, Marcel·li Domingo 1, 43007 Tarragona, Spain; magdalena.aguiló@urv.cat (M.A.); f.diaz@urv.cat (F.D.)

* Correspondence: xavier.mateos@urv.cat

Received: 29 September 2020; Accepted: 19 October 2020; Published: 24 October 2020



Featured Application: The Developed Raman Laser Gas Spectrometer is Suitable for Detection of Carbon Isotopologues of Methane and Carbon Dioxide in Human Exhalation.

Abstract: A compact Raman laser gas spectrometer is developed. It comprises a high-power green laser at 532.123 nm as an excitation source and a specially designed gas cell with an internal volume of less than 0.6 cm^3 that can withstand gas pressures up to 100 atm. The resolution of the spectrometer is $\sim 1\text{ cm}^{-1}$. The Raman spectra of chemically pure isotopically enriched carbon dioxide ($^{12}\text{CO}_2$, $^{13}\text{CO}_2$) and methane ($^{12}\text{CH}_4$, $^{13}\text{CH}_4$) gases are studied. The expected limit of detection (LOD) is less than 100 ppm for the isotopologues of CO_2 and less than 25 ppm for those of CH_4 (at a gas pressure of 50 atm.), making the developed spectrometer promising for studying the sources of emissions of greenhouse gases by resolving their isotopologue composition. We also show the suitability of the spectrometer for Raman spectroscopy of human exhalation.

Keywords: Raman laser spectrometer; carbon isotopes; greenhouse gases; carbon dioxide; methane; human exhalation

1. Introduction

Nowadays, the concentration of greenhouse gases (such as carbon dioxide (CO_2), methane (CH_4), nitrous oxide (N_2O), etc.) in the atmosphere is increasing due to the anthropogenic emissions. Thus, there is a need to determine the anthropogenic contribution against the natural background and to recognize emissions from various industries [1–3]. One possibility for doing this is via the carbon isotope (^{12}C and ^{13}C) ratio measurements of carbon dioxide (CO_2) and methane (CH_4) in the atmospheric air [4,5].

So far, the isotope ratio Raman spectroscopy of CO_2 has been addressed in several research works. In [6], the authors have found a way for determining the isotope-delta values (the relative difference of

isotope ratios with respect to the reference material) $\delta^{13}\text{C}$ using micro-Raman spectroscopy. A technique for monitoring $^{13}\text{CO}_2$ by cavity-enhanced Raman spectroscopy was developed in [7]. Quantitative analysis of carbon isotopic composition in CO_2 with the estimation of the measurement uncertainty was performed in [8]. A detailed experimental and theoretical study on isotopic surface-enhanced Raman spectroscopy was done in [9].

Defining the isotopic composition of greenhouse gases helps to constrain global budgets and to study sink and source processes [10]. CH_4 is an important anthropogenic and natural greenhouse gas and, moreover, it participates in atmospheric chemistry through its reaction with the hydroxyl radical [11]. Since individual CH_4 sources have characteristic isotope signatures, carbon and hydrogen isotope ratios of CH_4 (e.g., $\delta^{13}\text{C}-\text{CH}_4$) have been useful in constraining the global methane budget [12].

By precisely measuring the ratio of ^{13}C to ^{12}C , one is able to determine the source of methane [13]. The individual values depend on the mechanisms of the CH_4 formation and consumption prior to its release into the atmosphere. It was shown [14] that it is possible to accurately measure the methane content in natural gases using Raman spectroscopy. The results of this work show the possibility of isotope-ratio analysis of methane.

Nowadays, isotope ratio measurement systems based on optical spectrometers are used because of several advantages. The first one is the fundamental possibility to distinguish the isotopologues (molecules that differ only in their isotope composition) with the same molecular weight but different isotopic composition such as $^{16}\text{O}^{13}\text{C}^{16}\text{O}$ and $^{16}\text{O}^{12}\text{C}^{17}\text{O}$ (both representing carbon dioxide) [15]. Second, it is possible to perform calibration-free absolute measurements of isotopologues based on ab initio calculations of line intensities [16]. This is a relevant possibility in the metrology of isotope ratios because the International Committee for Weights and Measures (CIPM) encourages the development of absolute isotope ratio measurement values for reference materials [17]. Third, such systems are relatively easy to use, field deployable and low cost. They require no complicated sample preparation, provide real-time data, and allow for in situ monitoring with a spectroscopic selectivity. The disadvantage of the isotope ratio optical spectrometers compared to mass spectrometers is still low accuracy [18].

Raman spectroscopy has advantages over traditional methods in the analysis of pure isotopologues. Due to different selection rules, Raman spectroscopy can detect even diatomic homonuclear molecules such as O_2 or N_2 [19–22]. The development of Raman-based gas analyzers was presented in several papers [23,24]. A system for analysis of mixtures of CO and H_2 (synthesis gas) was proposed in [25]. The Purcell enhanced Raman scattering (PERS) device was used for isotopic gas analysis in [26]. A Raman analyzer for sensitive natural gas composition analysis was described in [27]. The main limitation is the low intensity of Raman scattering from gases. So far, the application of Raman spectroscopy for routine trace gas analysis has not found widespread use due to the inherent weakness of Raman transitions and it was mainly employed in condensed phases [28]. The above-mentioned limitation can be overcome by using intense excitation beams and high-pressure gas cavities. For the reliable $^{13}\text{C}/^{12}\text{C}$ ratio measurements, it is critical to calibrate the instruments. The preparation of calibration gas mixtures requires the analysis of the parent gases, such as pure $^{12}\text{CO}_2$ and $^{13}\text{CO}_2$ [29].

In the present work, we report on the method of quantitative analysis of $^{12}\text{CO}_2$, $^{13}\text{CO}_2$, $^{12}\text{CH}_4$ and $^{13}\text{CH}_4$ greenhouse gases based on Raman laser gas spectroscopy.

2. Materials and Methods

This study is dedicated to the development of a compact Raman laser gas spectrometer suitable for the analysis of gases under high pressures. The details of the spectrometer are described in Section 3.

The isotopically enriched carbon dioxide ($^{12}\text{CO}_2$, $^{13}\text{CO}_2$) and methane ($^{12}\text{CH}_4$ and $^{13}\text{CH}_4$) gases were studied. The CO_2 gases were provided by PA EXP, Ltd. (Russia) and the CH_4 ones by Cambridge Isotope Laboratories (USA). The chemical purity (CP) and carbon isotopic enrichment (δC) of the studied gases are specified in Table 1 (provided by the suppliers). The chemical purity shows the molar content of the main gas component and equals to 100% minus the total content of impurities (e.g., N_2 ,

O₂, Ar, CO, etc.). It is measured by gas chromatography–mass spectrometry (GC–MS). The carbon isotopic enrichment shows the content of the target isotopologue in the main gas component and it is measured by isotope-ratio mass spectrometry (IRMS). The gas temperature was 293 K.

Table 1. Chemical purity (CP) and carbon isotopic enrichment (δC) of the studied carbon dioxide and methane gases.

Gas	CP, %	δC , %
¹² CO ₂	>99.987	99.992
¹³ CO ₂	>99.994	99.57
¹² CH ₄	>99.5	>99.99
¹³ CH ₄	>99	>99.9

This work also includes the study of human exhalation. All subjects gave their informed consent for inclusion before they participated in the study. The study was conducted in accordance with the Declaration of Helsinki, and the protocol was approved by the Ethics Committee of ITMO University (project RFMEFI57518X0180).

3. Raman Laser Spectrometer

3.1. Excitation Source

The scheme of the spectrometer is shown in Figure 1. As the excitation source, we employed a continuous-wave diode-pumped solid-state laser (MSL-R-532, CNI-Lasers) emitting ~5 W of linearly polarized output at a wavelength of 532.123 nm with a full-angle divergence of 1.5 mrad, the beam quality parameter $M^2_{x,y} < 1.1$ (TEM₀₀ mode) and a laser linewidth of <1 pm (~0.03 cm⁻¹). The excitation beam was expanded using a ×7 Vega laser beam expander ($\lambda = 532$ nm, Edmund Optics) and focused into the gas cell using a specially designed doublet lens with a focal length $f = 55.9$ mm with both sides coated in antireflection (AR) coating at 532 nm. The measured spot size in the focus was less than 10 μ m (diameter, as measured by the optical knife method). The peak on-axis laser intensity was then about ~10 MW/cm². More details about the focusing system can be found elsewhere [30].

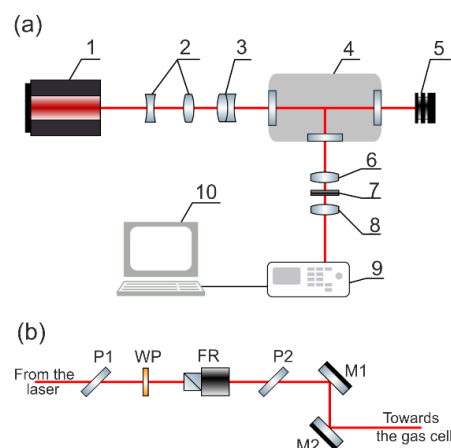


Figure 1. (a) Scheme of the Raman gas spectrometer: 1—excitation laser, 2—lens expander, 3—focusing lens, 4—gas cell, 5—laser radiation absorber, 6—collecting lens, 7—notch filter, 8—focusing lens, 9—spectrometer, 10—computer; (b) system for attenuation and optical alignment of the laser beam: P1 and P2—polarizers, WP—half-wave plate, M1, M2—highly reflective (HR) mirrors.

Prior to the beam expanding system, we installed a system based on a pair of crossed polarizers (P1 and P2) and a $\lambda/2$ waveplate and a Faraday rotator placed between them. It prevented back-scattered

light from damaging the excitation laser. In addition, a pair of flat highly reflective (HR) mirrors was used to precisely align the focal spot position in the gas cell, Figure 1b.

3.2. High-Pressure Gas Cell

A special gas cell made of titanium was developed, as shown in Figure 2. It was designed to work with gases in a limited volume with high pressure. The internal volume was only 0.57 cm^3 . To prevent reflections and light scattering, the internal surfaces of the gas cell were coated with an anti-glare enamel. The two optical windows for the excitation and scattered beams were made of K8 optical glass. The detection was at 90° to the optical axis of the laser beam. The gas cell can withstand pressures up to $\sim 100 \text{ atm}$. Note that CO_2 passes from the gaseous to liquid phase at a pressure of $\sim 60 \text{ atm}$.

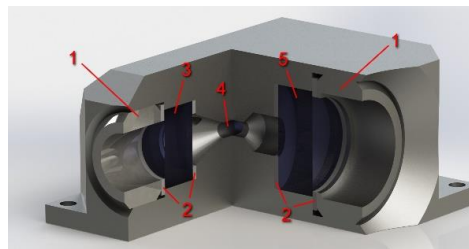


Figure 2. The scheme of the high-pressure gas cell: 1—nut rings, 2—polytetrafluoroethylene (PTFE) gaskets, 3—input window for passing the excitation light, 4—useful volume for the studied gas, 5—output window for collection of the scattered light.

The thickness of the optical windows was determined based on the calculations of the stress and displacement fields in the windows using the SolidWorks software, as shown in Figure 3a–d. The ultimate stress for both windows was assumed to be below the elastic limit of the K8 glass, $\sim 40 \text{ MPa}$, as shown in Figure 3e. Under these conditions, the minimum thickness of the windows is 8 mm with a deviation from flatness of $2 \mu\text{m}$ when exposed to a pressure of 100 atm. We have selected the thickness of 8 mm for both windows. The clear aperture (diameter) of the windows was $\sim 10 \text{ mm}$ (for the excitation beam) and 15 mm (for the scattered light). The input window was AR coated for 532 nm and the output one for 420–680 nm. The calculated fraction of the collected Raman signal determined by the geometry of the gas cell is 11%.

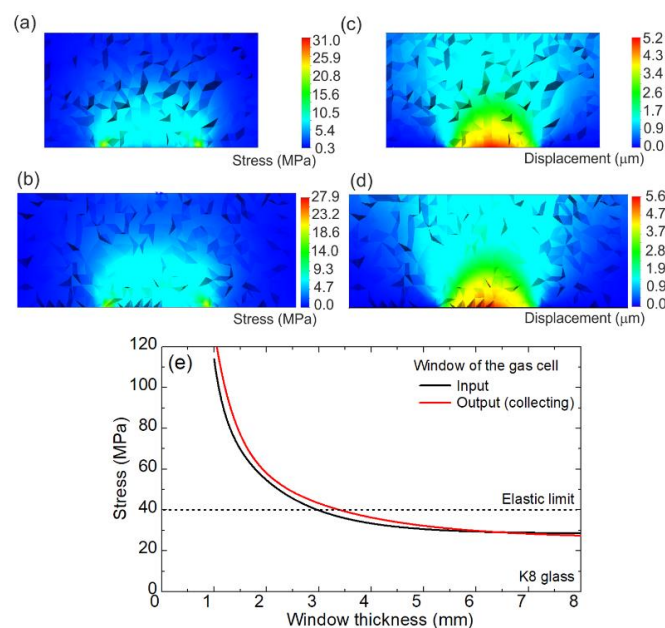


Figure 3. (a–d) Simulation of (a,b) the stress field, σ , and (c,d) the field of total displacements, u ,

in (a,c) the input window of the gas cell and (b,d) the output window used for collection of the scattered light. The gas pressure is 100 atm; (e) calculated maximum stress in the window vs. its thickness, the dashed line represents the elastic limit of the K8 glass (the window material). The grain structure in (a–d) represents the mesh used in the simulations.

The gas cell was equipped with a gas inlet and an outlet. First, a backing vacuum pump was connected to the outlet valve and the cell was evacuated to the pressure of 10^{-3} mm Hg. Then, the inlet valve was opened and the cell was filled in with the studied or reference gas. After the measurement, we released the gas into the evacuation system through the outlet valve.

3.3. Spectrometer

The scattered light was collected using an achromatic doublet lens ($f = 55.9$ mm) AR-coated for 420–680 nm. The Rayleigh scattered light was filtered out using a pair of notch filters (attenuation at 532 nm: $\times 10^{-12}$). Another achromatic doublet lens ($f = 80.6$ mm) was used to reimaged the scattered light at the input slit of the spectrometer. It had the same AR coating as for the collecting lens.

The spectrometer was based on a Czerny–Turner scheme. A diffraction grating with 1800 grooves per mm with a blazing wavelength of 500 nm was used. Its spectral efficiency at 330–860 nm exceeded 40%. The linear dispersion of the system was 1.52 nm/mm and the spectral resolution (the instrumental linewidth, full width at half maximum (FWHM)) was 0.05 nm. The reproducibility of the wavelength setting was 0.03 nm. To find a compromise between the spectral resolution and the signal-to-noise (SNR) ratio, the width of the entrance slit was ~ 20 μm during the experiments. For detecting the spectra, we used a complementary metal–oxide–semiconductor (CMOS) camera (Hamamatsu) with a 2048×122 pixel² grid (pixel size: 12×12 μm). It was cooled by a Peltier element to -40 °C. The exposure time varied from 10 μs up to 10 min. The projected spectral range was as long as 35 nm (0.017 nm per pixel). It was possible to shift this range within the interval 530–635 nm. More details can be found in [31].

The wavelength grading was performed using an Hg–He arc-discharge spectral lamp (DRGS-12). The calibration of the Raman spectrometer was performed using a certified reference material of toluene with a known Raman spectrum [32]. The determined relative standard deviation (Δ_{rel}) between the measured and standard peak Raman shifts of toluene was $<0.01\%$ for the range of Raman shifts of $1000\text{--}3300$ cm^{-1} (for $\lambda_{\text{exc}} = 532.123$ nm). The spectral resolution of the spectrometer was ~ 1 cm^{-1} (the instrumental linewidth, FWHM). The measurements were performed at room temperature (293 K).

4. Spectroscopy of $^{12}\text{C}/^{13}\text{C}$ Isotopologues

The study of greenhouse gas mixtures containing the gases of interest (i.e., carbon dioxide and methane) requires a preliminary study of the reference gases with high chemical and isotopic purity.

The Raman spectra of the carbon isotopologues of carbon dioxide and methane are known. Here, we briefly describe and interpret the measured spectra.

The CO_2 molecule is linear and centrosymmetric. The Raman spectrum of CO_2 , see Figure 4a, contains two intense and sharp Q-branches, which form the diad ν_1 (1388/1370 cm^{-1}) and $2\nu_2$ (1285/1266 cm^{-1}) for the $^{12}\text{C}/^{13}\text{C}$ containing molecules, respectively [33]. Adjacent to these lines, there are much weaker ones assigned as $\nu_1 + \nu_2 - \nu_2$ (1410 cm^{-1} for ^{12}C , for ^{13}C , it overlaps with the ν_1 line) and $3\nu_2 - \nu_2$ (1266/1248 cm^{-1} for $^{12}\text{C}/^{13}\text{C}$, respectively). The easiest attribution of the carbon isotopologues of CO_2 is according to the ν_1 and $2\nu_2$ diad, the wavenumber shift between the corresponding lines for the $^{12}\text{CO}_2$ and $^{13}\text{CO}_2$ molecules is $\sim 18\text{--}19$ cm^{-1} . The Raman lines of isotopologues of carbon dioxide are easily detectable even at low gas pressure (1 atm.) using isotopically-enriched gases.

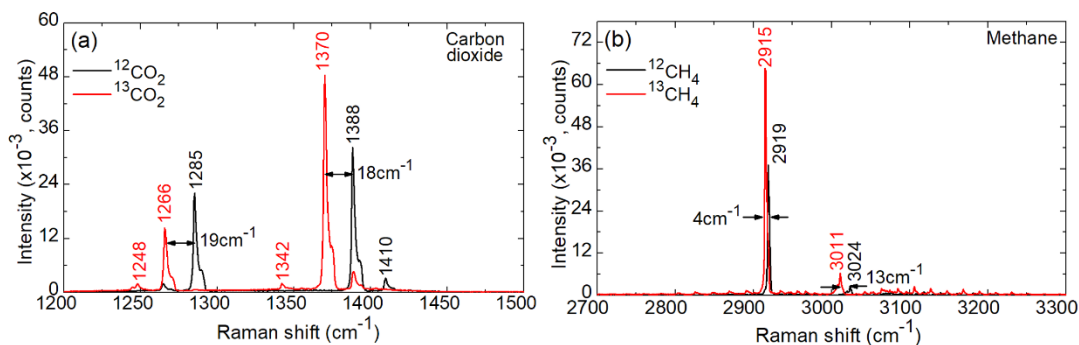


Figure 4. Raman spectra of isotopically enriched (a) carbon dioxide ($^{12}\text{CO}_2$ and $^{13}\text{CO}_2$) and (b) methane ($^{12}\text{CH}_4$ and $^{13}\text{CH}_4$) gases. The excitation wavelength $\lambda_{\text{exc}} = 532.123$ nm, the resolution is ~ 1 cm^{-1} . Gas pressure: 1 atm. Exposure time: 60 s.

The Raman spectra of the $^{12}\text{CH}_4$ isotopologue have been systematically studied. Much less information is present about the second most abundant natural isotopologues, $^{13}\text{CH}_4$ [34]. Only recently have several studies focused on filling in this gap [35]. CH_4 has tetrahedral symmetry (point group T_d) with four normal modes of vibration. They are labeled by irreducible representations of the T_d point group. The fundamental frequencies exhibit a simple relation, $\nu_1(A_1) \approx \nu_3(F_2) \approx 2\nu_2(E) \approx 2\nu_4(F_2)$. It leads to the so-called polyad structure in the Raman and infrared (IR) spectra [36]. A polyad P_n gathers all vibrational states (ν_1, ν_2, ν_3 and ν_4) satisfying the condition $n = 2(\nu_1 + \nu_3) + \nu_2 + \nu_4$, where ν_i are the vibrational quantum numbers for i -th ($i = 1, 2, 3, 4$) mode. Each set of $\{\nu_i\}$ defines a vibrational level. The pentad P_2 corresponds to five vibrational levels: $2\nu_4, \nu_2 + \nu_4, 2\nu_2, \nu_1$ and ν_3 . The lines in the Raman spectra corresponding to the pentad of methane are observed at ~ 3000 cm^{-1} and they can be used for detection of isotopologues of CH_4 .

The Raman spectra of isotopologues of methane around ~ 3000 cm^{-1} have a rich structure due to the complex vibration–rotation polyad interaction. The most intense line is observed at ~ 2919 cm^{-1} ($^{12}\text{CH}_4$) and 2915 cm^{-1} ($^{13}\text{CH}_4$) and is assigned as ν_1 . The isotope wavenumber shift is only ~ 4 cm^{-1} . This line is well detected even at low gas pressure and short exposure, as shown in Figure 4b. Other prominent lines are those at ~ 3024 cm^{-1} ($^{12}\text{CH}_4$) and 3011 cm^{-1} ($^{13}\text{CH}_4$), showing higher isotope wavenumber shift whilst showing much lower intensity.

The spectra from Figure 4 were analyzed to determine the limit of detection (LOD) for each of the gases, as shown in Table 2.

Table 2. Analysis ^a of the sensitivity of the Raman gas spectrometer according to the study of chemically pure isotopically enriched carbon dioxide and methane gases.

Parameter	$^{12}\text{CO}_2$	$^{13}\text{CO}_2$	$^{12}\text{CH}_4$	$^{13}\text{CH}_4$
ν , cm^{-1}	1388	1370	2919	2915
I_{signal} , counts	7630	13754	37487	64654
I_{noise} , counts	382	229	523	311
(<i>r.m.s.</i>) _{noise} , counts	28	27	30	28
ΔI_{signal} , counts	7248	13525	36964	64343
LOD (1 atm.), %	1.1731	0.5952	0.2428	0.1303
LOD (50 atm.), %	0.0227	0.0119	0.0049	0.0026
LOD (50 atm.), ppm	227	119	49	26
LOD (50 atm., 300 s), ppm	95	50	20	11

^a The Raman spectra are shown in Figure 4, gas pressure: 1 atm., exposure time: 60 s. The estimated limit of detection (LOD) values for the pressure of 50 atm. are according to Figure 5. The error in the specified LOD values is 14%. The estimated values are given in *italics*.

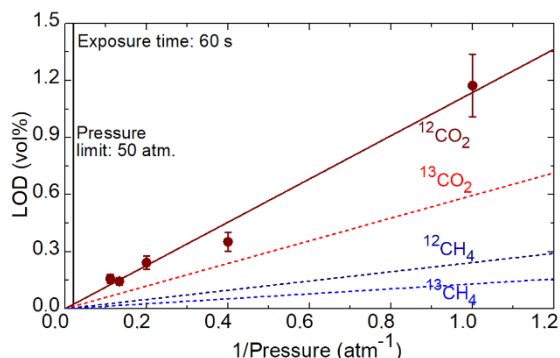


Figure 5. Limit of detection (LOD) of chemically pure isotopically enriched carbon dioxide and methane gases vs. inverse of the gas pressure: *symbols*: experimental data for $^{12}\text{CO}_2$ using the 1388 cm^{-1} Raman line, *solid line*—their linear fit, *dashed lines*—interpolation for other gases according to the measurement at 1 atm. Exposure time: 60 s.

First, the Raman intensity at the characteristic Raman shift (ν) was determined both for the signal (I_{signal}) and noise (I_{noise}) yielding the useful signal, $\Delta I_{\text{signal}} = I_{\text{signal}} - I_{\text{noise}}$. The room mean square value of the noise, $(r.m.s.)_{\text{noise}}$, was also determined. The noise analysis was performed using the spectra of isotopically enriched gases in the wavenumber range free of Raman lines covering about $\sim 1000\text{ cm}^{-1}$. The LOD is:

$$\text{LOD}_{\text{vol}\%} = X_{\text{vol}\%} \frac{3(r.m.s.)_{\text{noise}}}{\Delta I_{\text{signal}}} \quad (1)$$

here, $X_{\text{vol}\%}$ is the volume fraction of the studied gas, which is close to 100% for chemically pure isotopically enriched gases, cf. Table 1. The results on the LOD are shown in Table 2, being expressed both in vol% and parts per million (ppm), $\text{LOD}_{\text{ppm}} = 10^4 \times \text{LOD}_{\text{vol}\%}$.

The upper limit for the error in the LOD estimation was determined by analyzing 10 repetitive measurements for the $^{12}\text{CH}_4$ gas. The maximum deviation from the average LOD value was $\sim 14\%$.

The LOD can be decreased in two ways. One is the increase in the gas pressure. The limit of detection is proportional to inverse of the gas pressure p , $\text{LOD} \sim 1/p$, see Equation (1). Indeed, the useful Raman signal of a gas is proportional to the gas pressure [37], while the noise level is mostly determined by the detector and thus is independent of the pressure. To confirm this, we have measured the Raman spectra of chemically pure isotopically enriched $^{12}\text{CO}_2$ gas at various gas pressures in the range of 1–9 atm., keeping the same exposure time of 60 s. The resulting LOD values (according to the 1388 cm^{-1} Raman line) are shown in Figure 5. The data agree well with the $\text{LOD} \sim 1/p$ law, yielding an estimation of the limit of detection at the maximum available gas pressure (50 atm.) of 227 ppm (for 60 s exposure). Note that particularly for CO_2 at high pressures (>50 atm.), it was pointed out in [10] that the exponential law better describes the dependence of the Raman signal on the gas pressure. Further studies are thus required at such elevated pressures.

Using the data measured at 1 atm., we interpolated the dependences for other gases, as shown in Figure 5 by dashed lines. The corresponding LOD (50 atm.) values are listed in Table 2. In particular, for methane, they are as low as 49 ppm ($^{12}\text{CH}_4$) and 26 ppm ($^{13}\text{CH}_4$).

Another possible way to improve the LOD is to increase the exposure time, however this approach is of limited use for applications where relatively fast characterization is needed. As an example, we studied the $^{13}\text{CH}_4$ gas at a fixed pressure of 1 atm. and an exposure time Δt in the range of 1–60 s. The Raman spectra obtained for $\Delta t = 1\text{--}30$ s are presented in Figure 6a. Longer exposures allow the observation of weak spectral details of the $^{13}\text{CH}_4$ pentad.

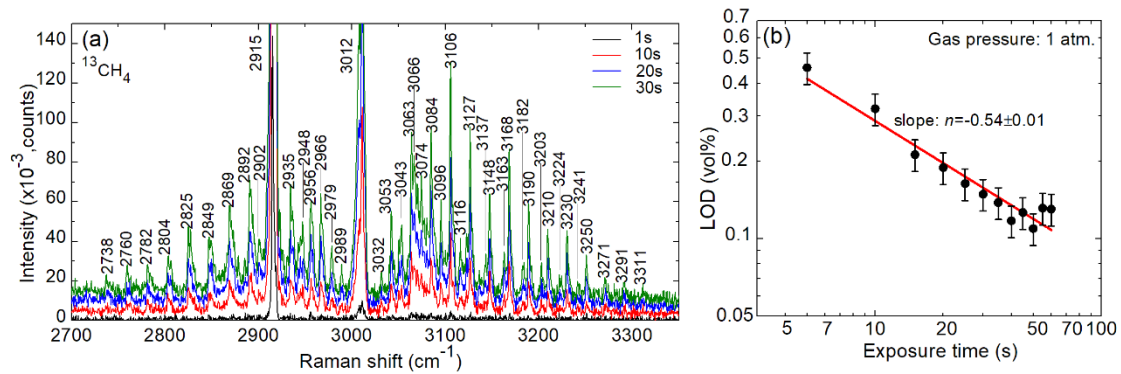


Figure 6. (a) Raman spectrum of high-purity (>99%) isotopically-enriched (>99.9% ^{13}C) $^{13}\text{CH}_4$ gas. The excitation wavelength $\lambda_{\text{exc}} = 532.123$ nm, the resolution is ~ 1 cm^{-1} . Gas pressure: 1 atm. Exposure time Δt : 1–30 s; (b) double-logarithmic plot of LOD vs. the exposure time, *symbols*: experimental data, *line*: linear fit according to Equation (2). Gas pressure: 1 atm.

The dependence of LOD on the exposure time Δt , plotted in a double-logarithmic scale is shown in Figure 6b. From statistics, it is known that the root mean square (r.m.s.) of an average value is reduced by a factor of $N^{-0.5}$ with respect to that of a single measurement, where N is the number of measurements, which are averaged. Thus, if $\Delta t_0 = 1$ s measurement yields a limit of detection of LOD_0 , any longer measurement with $\Delta t = s \times \Delta t_0$ can be represented as a set of s elementary measurements with $\text{LOD}(\Delta t) = \text{LOD}_0 \times s^{-0.5} = \text{LOD}_0 \times (\Delta t/\Delta t_0)^{-0.5}$. By plotting Figure 6b in a double-logarithmic scale and fitting the experimental points by a linear function, we obtain the slope n of the dependence:

$$\text{LOD}(\Delta t) = \text{LOD}_0 \left(\frac{\Delta t}{\Delta t_0} \right)^{-n} \quad (2)$$

In our case, $n = -0.54 \pm 0.01$, which agrees well with the theoretical considerations.

By considering both the effects of the increased gas pressure ($p = 50$ atm.) and the exposure time ($\Delta t = 300$ s), we obtained lower-limit estimations of LOD for all four studied gases, cf. Table 2, i.e., <100 ppm for the isotopologues of carbon dioxide and <25 ppm for those of methane.

5. Towards Applications: Human Exhalation

Raman spectroscopy is well suited for the simultaneous detection of various gases in the analysis of human respiration [38]. Natural carbon isotopes (^{12}C and ^{13}C) present in human breath can be used to identify various diseases. Carbon isotopes in exhaled CO_2 can be a valuable real-time biomarker of cachexia [39] (depletion of the body), associated with the acute phase of the reaction caused by endotoxemia (accumulation of toxic substances in the body). The acute phase reaction causes shifts in stable carbon isotopes in exhaled CO_2 , which can be used to monitor nutrient metabolism. Isotope mass spectrometry (IRMS) exists to determine CO_2 carbon isotopes in human respiration [40]. This method has high accuracy, sensitivity and stability, but it is rather complex, expensive and requires large expenditures on equipment and staff training. There is a less expensive way to detect CO_2 isotopes using an isotope-selective non-dispersive infrared spectrometer (NDIRS) [41], but it is only suitable for simple breath tests where a small number of samples is required, for example, to detect diseases of the gastrointestinal tract and detect *Helicobacter pylori* [42]. This is due to a decrease in the correlation of repeated measurements with longer series of measurements.

A Raman spectrum overview of a human exhalation measured at ambient pressure (1 atm.) is shown in Figure 7a. It shows several intense Raman peaks at 1285 and 1388 cm^{-1} (both $^{12}\text{CO}_2$), 1556 cm^{-1} (O_2), 2328 cm^{-1} (N_2) and 2919 cm^{-1} ($^{12}\text{CH}_4$). By focusing on the spectral range around ~ 1300 cm^{-1} and applying longer exposure (600 s), we were able to clearly resolve the Raman lines assigned to the isotopologues of carbon dioxide ($^{12}\text{CO}_2$ and $^{13}\text{CO}_2$). The spectral position of the

lines and the isotopic wavenumber shifts agree well with the data for isotopically enriched gases, cf. Figure 4.

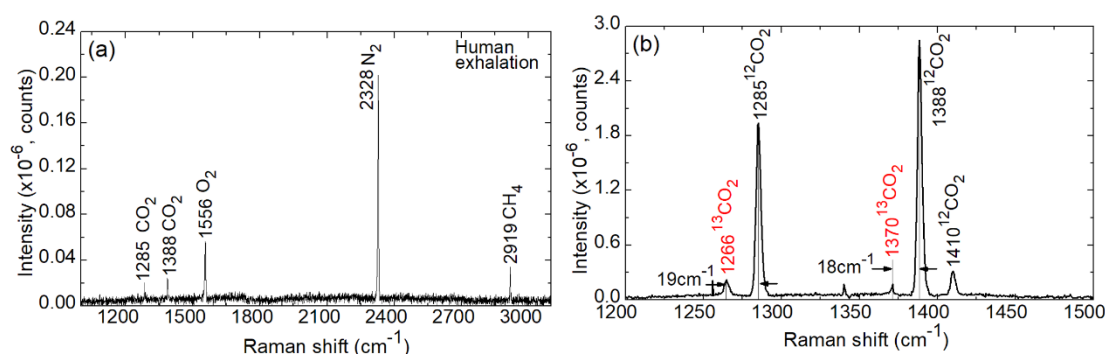


Figure 7. Raman spectrum of the human breath (exhalation): (a) an overview spectrum; (b) a close view of the $^{12}\text{CO}_2/^{13}\text{CO}_2$ lines. The excitation wavelength $\lambda_{\text{exc}} = 532.123$ nm, the resolution is ~ 1 cm^{-1} . Gas pressure: 1 atm. Exposure time: (a) 30 s, (b) 600 s.

The Raman spectra of isotopologues of carbon dioxide were analyzed from the point of view of the LOD in order to confirm the values obtained with the isotopically enriched gases, see Figure 4. Note that the LOD can be calculated for any gas in a gas mixture if its volume fraction $X_{\text{vol}}\%$ is known, see Equation (1). The volume fractions of $^{12}\text{CO}_2$ and $^{13}\text{CO}_2$ gases in human exhalation depends on different factors, e.g., the time between breathing in and out [43,44]. We used the mean values of 4 vol% $^{12}\text{CO}_2$ and 0.04 vol% $^{13}\text{CO}_2$. Based on these volume fractions and the measured Raman spectra, as shown in Figure 7b, we have determined the LOD to be 225 ppm ($^{12}\text{CO}_2$) and 75 ppm ($^{13}\text{CO}_2$) at a gas pressure of 1 atm. and an exposure time of 600 s. These values agree well with the analysis performed in Table 2, considering the difference in the exposure time.

6. Conclusions

To conclude, we have developed a sensitive and compact Raman laser spectrometer suitable for analyzing gas mixtures containing relevant greenhouse gases such as carbon dioxide and methane. In particular, it is capable of identifying the contributions of carbon isotopologues, such as $^{12}\text{CO}_2/^{13}\text{CO}_2$ and $^{12}\text{CH}_4/^{13}\text{CH}_4$. The features of the developed spectrometer result in a specially designed gas cell with the following advantages: (i) it can withstand high gas pressures (up to 100 atm.), (ii) it has a relatively small internal volume of ~ 0.6 cm^3 , relaxing the requirements for sample preparation, and (iii) together with the optical scheme of the spectrometer, it ensures good collection efficiency for the scattered light and, thus low limits of detection (LODs) for the studied gases. By studying isotopically-enriched $^{12}\text{CO}_2/^{13}\text{CO}_2$ and $^{12}\text{CH}_4/^{13}\text{CH}_4$ gases, we estimated easily accessible LODs of less than 100 ppm for the isotopologues of carbon dioxide and less than 25 ppm for those of methane. We also show the proof-of-the-concept of the suitability of the developed spectrometer for studying human exhalation.

Further work will focus on developing a gas analyzer using calibrated gas mixtures. Such Raman gas spectrometers and gas analyzers are promising for studies of sources of pollution in the atmosphere, combustion processes and human exhalation.

Potentially, the developed Raman gas spectrometer can be used for analyzing virus structures in human exhalation.

Author Contributions: Conceptualization and methodology, E.P., I.C., A.K. (Artem Kharitonov), P.C. and P.L.; validation, A.P. and A.D.; formal analysis, V.K.; investigation, V.V., I.C., E.P., A.P., A.D. and V.K.; data curation, A.K. (Anton Kovalev); writing—original draft preparation, I.C., K.G.; writing—review and editing, P.L., M.A. and F.D.; visualization, K.G. and V.K.; supervision, V.V.; project administration, V.V. and X.M.; funding acquisition, V.V. All authors have read and agreed to the published version of the manuscript.

Funding: This research was funded by Ministry of Education and Science of Russian Federation, grant number RFMEFI57518X0180.

Conflicts of Interest: The authors declare no conflict of interest.

References

1. Rieker, G.B.; Giorgetta, F.R.; Swann, W.C.; Kofler, J.; Zolot, A.M.; Sinclair, L.C.; Baumann, E.; Cromer, C.; Petron, G.; Sweeney, C.; et al. Frequency-comb-based remote sensing of greenhouse gases over kilometer air paths. *Optica* **2014**, *1*, 290–298. [CrossRef]
2. Ghosh, P.; Brand, W.A. Stable isotope ratio mass spectrometry in global climate change research. *Int. J. Mass Spectrom.* **2003**, *228*, 1–33. [CrossRef]
3. Schneider, S.H. Detecting climatic change signals: Are there any “fingerprints”? *Science* **1994**, *263*, 341–347. [CrossRef] [PubMed]
4. Stevens, C.M.; Rust, F.E. The carbon isotopic composition of atmospheric methane. *J. Geophys. Res. Oceans* **1982**, *87*, 4879–4882. [CrossRef]
5. Monteil, G.A.; Houweling, S.; Dlugokenky, E.J.; Maenhout, G.; Vaughn, B.H.; White, J.W.C.; Rockmann, T. Interpreting methane variations in the past two decades using measurements of CH₄ mixing ratio and isotopic composition. *Atmosph. Chem. Phys.* **2011**, *11*, 9141–9153. [CrossRef]
6. Li, J.J.; Li, R.X.; Dong, H.; Wang, Z.H.; Zhao, B.S.; Wang, N.; Cheng, J.H. Carbon isotopic compositions in carbon dioxide measured by micro-laser Raman spectroscopy. *J. Appl. Spectrosc.* **2017**, *84*, 237–241. [CrossRef]
7. Keiner, R.; Frosch, T.; Massad, T.; Trumbore, S.; Popp, J. Enhanced Raman multigas sensing—A novel tool for control and analysis of ¹³CO₂ labeling experiments in environmental research. *Analyst* **2014**, *139*, 3879–3884. [CrossRef] [PubMed]
8. Li, J.; Li, R.; Zhao, B.; Guo, H.; Zhang, S.; Cheng, J.; Wu, X. Quantitative measurement of carbon isotopic composition in CO₂ gas reservoir by micro-laser Raman spectroscopy. *Spectrochim. Acta A Mol. Biomol. Spectrosc.* **2018**, *195*, 191–198. [CrossRef] [PubMed]
9. Zhang, M.; Zhao, L.B.; Luo, W.L.; Pang, R.; Zong, C.; Zhou, J.Z.; Ren, B.; Tian, Z.Q.; Wu, D.Y. Experimental and theoretical study on isotopic surface-enhanced Raman spectroscopy for the surface catalytic coupling reaction on silver electrodes. *J. Phys. Chem. C* **2016**, *120*, 11956–11965. [CrossRef]
10. Prinzhofer, A.; Battani, A. Gas isotopes tracing: An important tool for hydrocarbons exploration. *Oil Gas Sci. Technol.* **2003**, *58*, 299–311. [CrossRef]
11. Naik, V.; Voulgarakis, A.; Fiore, A.M.; Horowitz, L.W.; Lamarque, J.F.; Lin, M.; Prather, M.J.; Young, P.J.; Bergmann, D.; Cameron-Smith, P.J.; et al. Preindustrial to present-day changes in tropospheric hydroxyl radical and methane lifetime from the Atmospheric Chemistry and Climate Model Intercomparison Project (ACCMIP). *Atmosph. Chem. Phys.* **2013**, *13*, 5277–5298. [CrossRef]
12. Bergamaschi, P.; Schupp, M.; Harris, G.W. High-precision direct measurements of ¹³CH₄/¹²CH₄ and ¹²CH₃D/¹²CH₄ ratios in atmospheric methane sources by means of a long-path tunable diode laser absorption spectrometer. *App. Opt.* **1994**, *33*, 7704–7716. [CrossRef] [PubMed]
13. Bréas, O.; Guillou, C.; Reniero, F.; Wada, E. The global methane cycle: Isotopes and mixing ratios, sources and sinks. *Isot. Environ. Health S.* **2001**, *37*, 257–379. [CrossRef]
14. Petrov, D.V.; Matrosov, I.I. Raman gas analyzer (RGA): Natural gas measurements. *Appl. Spectrosc.* **2016**, *70*, 1770–1776. [CrossRef]
15. Prokhorov, I.; Kluge, T.; Janssen, C. A novel method of carbon dioxide clumped isotope analysis with tunable infra-red laser direct absorption spectroscopy. In Proceedings of the EGU General Assembly 2016, Vienna, Austria, 17–22 April 2016.
16. Polyansky, O.L.; Bielska, K.; Ghysels, M.; Lodi, L.; Zobov, N.F.; Hodges, J.T.; Tennyson, J. High-accuracy CO₂ line intensities determined from theory and experiment. *Phys. Rev. Lett.* **2015**, *114*, 243001. [CrossRef] [PubMed]
17. International Committee for Weights and Measures. Proceedings of Session I of the 104th Meeting (9–10 March 2015). Available online: <https://www.bipm.org/utis/en/pdf/CIPM/CIPM2015-I-EN.pdf> (accessed on 29 August 2020).

18. Van Geldern, R.; Nowak, M.E.; Zimmer, M.; Szizybalski, A.; Myrntinen, A.; Barth, J.A.; Jost, H.J. Field-based stable isotope analysis of carbon dioxide by mid-infrared laser spectroscopy for carbon capture and storage monitoring. *Anal. Chem.* **2014**, *86*, 12191–12198. [[CrossRef](#)] [[PubMed](#)]
19. Siberio-Pérez, D.Y.; Wong-Foy, A.G.; Yaghi, O.M.; Matzger, A.J. Raman spectroscopic investigation of CH₄ and N₂ adsorption in metal–organic frameworks. *Chem. Mater.* **2007**, *19*, 3681–3685. [[CrossRef](#)]
20. Keutel, D.; Seifert, F.; Oehme, K.L.; Asenbaum, A.; Musso, M. Evidence for negative cross correlations in vibrational dephasing in liquids: Isotropic Raman-line shift and width phenomena in isotopic mixtures of N₂ and O₂. *Phys. Rev. Lett.* **2000**, *85*, 3850. [[CrossRef](#)]
21. Cabaço, M.I.; Longelin, S.; Danten, Y.; Besnard, M. Transient dimer formation in supercritical carbon dioxide as seen from Raman scattering. *J. Chem. Phys.* **2008**, *128*, 074507. [[CrossRef](#)]
22. Musso, M.; Matthai, F.; Keutel, D.; Oehme, K.L. Critical Raman line shape behavior of fluid nitrogen. *Pure Appl. Chem.* **2004**, *76*, 147–155. [[CrossRef](#)]
23. Yan, D.; Popp, J.; Frosch, T. Analysis of fiber-enhanced Raman gas sensing based on Raman chemical imaging. *Anal. Chem.* **2017**, *89*, 12269–12275. [[CrossRef](#)] [[PubMed](#)]
24. Yu, A.; Zuo, D.; Wang, X. Optimization of parabolic cell for gas Raman analysis. *J. Raman Spectrosc.* **2019**, *50*, 731–740. [[CrossRef](#)]
25. Eichmann, S.C.; Weschta, M.; Kiefer, J.; Seeger, T.; Leipertz, A. Characterization of a fast gas analyzer based on Raman scattering for the analysis of synthesis gas. *Rev. Sci. Instrum.* **2010**, *81*, 125104. [[CrossRef](#)] [[PubMed](#)]
26. Petrak, B.; Cooper, J.; Konthasinghe, K.; Peiris, M.; Djeu, N.; Hopkins, A.J.; Muller, A. Isotopic gas analysis through Purcell cavity enhanced Raman scattering. *Appl. Phys. Lett.* **2016**, *108*, 091107. [[CrossRef](#)]
27. Sharma, R.; Poonacha, S.; Bekal, A.; Vartak, S.; Weling, A.; Tilak, V.; Mitra, C. Raman analyzer for sensitive natural gas composition analysis. *Opt. Eng.* **2016**, *55*, 104103. [[CrossRef](#)]
28. John, S.T.; Shaw, D.M.; Klug, D.D.; Patchkovskii, S.; Vankó, G.; Monaco, G.; Krisch, M. X-ray Raman spectroscopic study of water in the condensed phases. *Phys. Rev. Lett.* **2008**, *100*, 095502. [[CrossRef](#)]
29. Chubchenko, Y.K.; Konopel'ko, L.A. Development of a new type of reference standard for carbon isotopic composition. *Measur. Tech.* **2018**, *60*, 1228–1232. [[CrossRef](#)]
30. Vitkin, V.V.; Chubchenko, I.K.; Polischuk, A.V.; Kovalev, A.V.; Popov, E.E. Raman gas analyzer for detecting carbon isotopologues. *J. Physics: Conf. Ser.* **2019**, *1399*, 022033. [[CrossRef](#)]
31. Popov, E.; Polishchuk, A.; Grigorenko, K.; Chubchenko, I.; Vitkin, V. Raman detector of carbon isotopes. *Opt. Sens. Det. VI* **2020**, *11354*, 113542P. [[CrossRef](#)]
32. ASTM E1840-96. *Standard Guide for Raman Shift Standards for Spectrometer Calibration*; ASTM International: West Conshohocken, PA, USA, 1996.
33. Howard-Lock, H.E.; Stoicheff, B.P. Raman intensity measurements of the Fermi diad $\nu_1, 2\nu_2$ in ¹²CO₂ and ¹³CO₂. *J. Mol. Spectrosc.* **1971**, *37*, 321–326. [[CrossRef](#)]
34. Niederer, H.M.; Wang, X.G.; Carrington, T., Jr.; Albert, S.; Bauerecker, S.; Boudon, V.; Quack, M. Analysis of the rovibrational spectrum of ¹³CH₄ in the Octad range. *J. Mol. Spectrosc.* **2013**, *291*, 33–47. [[CrossRef](#)]
35. Niederer, H.M.; Albert, S.; Bauerecker, S.; Boudon, V.; Champion, J.P.; Quack, M. Global analysis of the infrared spectrum of ¹³CH₄: Lines in the region 0 to 3200 cm⁻¹. *CHIMIA Int. J. Chem.* **2008**, *62*, 273–276. [[CrossRef](#)]
36. Boudon, V.; Rey, M.; Loete, M. The vibrational levels of methane obtained from analyses of high-resolution spectra. *J. Quant. Spectrosc. Rad. Transf.* **2006**, *98*, 394–404. [[CrossRef](#)]
37. Gooijer, C.; Ariese, F.; Hofstraat, J.W. *Chemical Analysis: A Series of Monographs on Analytical Chemistry and Its Application*; John Wiley & Sons: New York, NY, USA, 2000.
38. Okita, Y.; Katagiri, T.; Matsuura, Y. A Raman cell based on hollow optical fibers for breath analysis. In *Optical Fibers and Sensors for Medical Diagnostics and Treatment Applications X*; International Society for Optics and Photonics: San Francisco, CA, USA, 2010; Volume 7559, p. 755908. [[CrossRef](#)]
39. Butz, D.E.; Cook, M.E.; Eghbalnia, H.R.; Assadi-Porter, F.; Porter, W.P. Changes in the natural abundance of ¹³CO₂/¹²CO₂ in breath due to lipopolysacchride-induced acute phase response. *Rapid Commun. Mass Spectrosc.* **2009**, *23*, 3729–3735. [[CrossRef](#)] [[PubMed](#)]
40. Braden, B.; Haisch, M.; Duan, L.P.; Lembcke, B.; Caspary, W.F.; Hering, P. Clinically feasible stable isotope technique at a reasonable price: Analysis of ¹³CO₂/¹²CO₂-abundance in breath samples with a new isotope selective-nondispersive infrared spectrometer. *Z. Gastroenterol.* **1994**, *32*, 675–678. [[PubMed](#)]

41. Barth, E.; Tugtekin, I.; Weidenbach, H.; Wachter, U.; Vogt, J.; Radermacher, P.; Adler, G.; Georgieff, M. Determination of $^{13}\text{CO}_2/^{12}\text{CO}_2$ ratio by IRMS and NDIRS. *Isot. Environ. Health S.* **1998**, *34*, 209–213. [[CrossRef](#)]
42. Koletzko, S.; Koletzko, B.; Haisch, M.; Hering, P.; Seeboth, I.; Hengels, K.; Braden, B. Isotope-selective non-dispersive infrared spectrometry for detection of *Helicobacter pylori* infection with ^{13}C -urea breath test. *Lancet* **1995**, *345*, 961–962. [[CrossRef](#)]
43. Normand, S.; Pachiaudi, C.; Khalfallah, Y.; Guilluy, R.; Mornex, R.; Riou, J.P. ^{13}C appearance in plasma glucose and breath CO_2 during feeding with naturally ^{13}C -enriched starchy food in normal humans. *Am. J. Clin. Nutr.* **1992**, *55*, 430–435. [[CrossRef](#)]
44. Schoeller, D.A.; Brown, C.; Nakamura, K.; Nakagawa, A.; Mazzeo, R.S.; Brooks, G.A.; Budinger, T.F. Influence of metabolic fuel on the $^{13}\text{C}/^{12}\text{C}$ ratio of breath CO_2 . *Biomed. Mass Spectrom.* **1984**, *11*, 557–561. [[CrossRef](#)]

Publisher's Note: MDPI stays neutral with regard to jurisdictional claims in published maps and institutional affiliations.



© 2020 by the authors. Licensee MDPI, Basel, Switzerland. This article is an open access article distributed under the terms and conditions of the Creative Commons Attribution (CC BY) license (<http://creativecommons.org/licenses/by/4.0/>).